Mol. BioSyst., 2009, DOI:10.1039/B903719E (Paper)

Retracted article: Shell-cross-linked stable multifunctional polymeric vesicles as magnetic resonance imaging contrast agents and drug nanocarriers

Xiaoqiang Yang[a], **Jamison J. Grailer**[b], **Srikanth Pilla**[a], **Douglas A. Steeber**[b], **Shaoqin Gong***[ac], **Yinghua Chen**[d] **and Guihua Chen**[d]

[a]*Department of Mechanical Engineering, University of Wisconsin-Milwaukee, Milwaukee, WI 53211, USA. E-mail: sgong@uwm.edu; Fax: +1-414-229-5946; Tel: +1-414-229-6958*

[b]*Department of Biological Sciences, University of Wisconsin-Milwaukee, Milwaukee, WI 53211, USA*

[c]*Department of Materials, University of Wisconsin-Milwaukee, Milwaukee, WI 53211, USA*

[d]*The Third Affiliated Hospital, Sun Yat-Sen University, Guangzhou 510630, P. R. China*

Received 25th February 2009, Accepted 23rd June 2009

First published on the web 28th July 2009

We, the named authors, hereby wholly retract this *Molecular BioSystems* article. Signed: Xiaoqiang Yang, Jamison J. Grailer, Srikanth Pilla, Douglas A. Steeber, Shaoqin Gong, Yinghua Chen and Guihua Chen, Milwaukee, USA, August 2009. Retraction endorsed by Michael Smith, Commissioning Editor. Retraction published 24th August 2009.

Introduction

Multifunctional nanomedicine is receiving considerable attention for its potential in drug delivery and molecular imaging applications.[1–3] This new nanomedicine paradigm allows for a highly integrated design that incorporates multiple functions such as cell targeting, imaging ultrasensitivity, and drug therapy within one system. Various nanoplatforms have been explored, including liposomes, micelles, nanocapsules, polymeric nanoparticles, solid lipid particles, and niosomes,[4–7] to simultaneously perform various important therapeutic or diagnostic functions.

To prepare multifunctional pharmaceutical nanocarriers, scientists have generally modified the nanoparticles chemically in order to simultaneously assemble a number of individual desirable properties on a single nanoparticle. The most important outcomes of such modifications include increased stability, prolonged blood circulation, optimized biodistribution, active targeting to the required pathological zone, responsiveness to local physiological stimuli, and the ability to serve as ultrasensitive imaging agents for various imaging modalities.

Several excellent reports on multifunctional drug delivery systems are available in the literature. Bae *et al.* improved their poly(ethylene glycol)-poly(L-histidine) pH-sensitive drug delivery system[8,9] by conjugating folic acid as tumor-targeting ligands to the pH-sensitive copolymer, thereby achieving the active tumor-targeting function. Such multifunctional drug nanocarriers can provide both enhanced cell uptake due to the incorporation of tumor-targeting ligands and enhanced intracellular drug release due to its pH sensitivity. Gao *et al.* reported the development of superparamagnetic polymeric micelles as a new class of magnetic resonance imaging (MRI) probes with remarkably high spin–spin (T_2) relaxtivity and sensitivity.[10] Furthermore, Gao *et al.* designed a tri-functional drug delivery system that provides specific targeting, pH

sensitivity, and image contrast by incorporating superparamagnetic iron oxide nanoparticles into a doxorubincin-loaded, cRGD-targeted, PEG-PLA micelle.[11] Meier *et al.* designed cross-linked polymeric vesicles based on polymerizable ABA triblock copolymers in order to increase their stability.[12]

This article describes the development of multifunctional polymeric vesicles with a double shell-cross-linked, ultra-stable structure for controlled drug delivery and enhanced MRI contrast (Scheme 1). This novel vesicle system has three key features. (1) The chemotherapeutic agent doxorubicin (DOX) hydrochloride was encapsulated into the inner aqueous core of the vesicle. In contrast to many types of DOX nanocarrier reported, such as polymeric micelles, it was not necessary to deprotonate DOX·HCl in order to obtain the hydrophobic DOX. DOX is a widely used anti-tumor therapeutic agent. (2) A large number of SPIO nanoparticles were encapsulated inside the hydrophobic membrane of the vesicle for ultrasensitive MRI detection. (3) The polymeric vesicle exhibited excellent stability due to the cross-linked structure in its inner and outer hydrophilic layers; thus, it can maintain its integrity *in vivo* despite significant dilution after intravenous injection. The cross-linked structure also can increase the half-time of circulation.[13] Without the cross-linked hydrophilic shells, the SPIO-DOX-loaded vesicles may disassemble *in vivo* when the concentration of the copolymers is below the critical micelle concentration. Once disassembled, the encapsulated agents, including SPIO nanoparticles and DOX, will release into the bloodstream before reaching the tumor tissue; therefore, any potential advantages that may be provided by the vesicle nanocarrier, including the passive tumor-targeting ability attributed to the enhanced permeability and retention (EPR) effect, will not be realized. Moreover, a sudden release of a high concentration of drugs may also cause some serious toxicity problems.

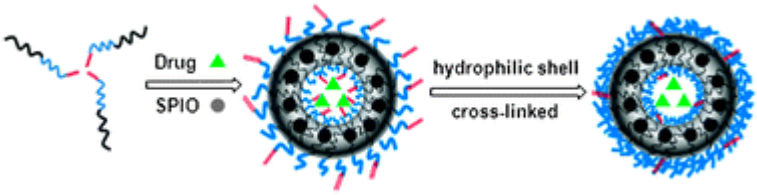

Scheme 1 Schematic illustration of the shell-cross-linked SPIO-DOX-loaded vesicle formation.

Experimental

Materials

D,L-lactide was purchased from Sigma-Aldrich Co. (USA) and recrystallized twice from ethyl acetate before use. Stannous(II) octoate ($Sn(Oct)_2$, from Sigma-Aldrich) was used as received. Allyl alcohol (from Fisher Scientific, Inc., USA) was purified by vacuum distillation over calcium hydride (CaH_2). Tetrahydrofuran (THF, from Sigma-Aldrich) was dried by refluxing over a sodium–potassium alloy and distilled under dry N_2. In addition, 18-crown-6 (from Fisher Scientific) was vacuum-dried overnight at 46 °C. Potassium persulfate ($K_2S_2O_8$) and ethylene oxide (EO) were purchased from Fisher Scientific and used as received. Phenyl ether (99%), benzyl ether (99%), 1,2-hexadecanediol (97%), oleic acid (90%), oleylamine(>70%), and iron(III) acetylacetonate were purchased from Sigma-Aldrich. All organic solvents are of analytic grade. Phosphate buffered solutions (PBS, pH7.4) and acetate buffered solutions (ABS, pH5.0) were prepared in our laboratory. RPMI-1640 was purchased from Gibco BRL (USA). The mouse mammary carcinoma, 4T1 (ATCC), was cultured in RPMI medium supplemented with 10% fetal calf serum.

Measurements

First, ^{1}H NMR spectroscopy of the samples was recorded on a Bruker DPX 300 spectrometer and the molecular weight and polydispersity were determined by gel permeation chromatography (GPC) (Viscotek Corp., USA). Samples for transmission electron microscopy (TEM, Hitachi H-600) analysis were prepared by drying a dispersion of the particles on a copper grid coated with amorphous carbon. Subsequently, a small drop of phosphotungstic acid (PTA) solution (2 wt% in water) was added to the copper grid; after 30 s, the grid was blotted with filter paper. Dynamic light scattering (DLS) (Brookhaven BI-200SM laser scattering system) was used to study the size distribution of various polymeric vesicles (10 mg ml^{-1}). DLS experiments were performed at a 90 °C scattering angle and 25 °C.

Synthesis of diblock copolymer of allyl-terminated poly(ethylene glycol) and poly(D,L-lactide) (allyl-PEG-PDLLA)

The synthesis scheme for allyl-PEG-PDLLA is shown in Scheme 2. This copolymer was synthesized by sequential, multistep, anionic polymerization of EO and D,L-lactide in one pot using potassium alkoxide as an initiator. Briefly, a desired amount of EO was added slowly into an ice-cold flask containing anhydrous THF solution of potassium alkoxide under stirring. Afterwards, the EO ring-opening polymerization was conducted at -5 °C for 24 h and then at room temperature for three days to ensure a thorough conversion of EO. Subsequently, a pre-determined amount of D,L-lactide was injected into the reaction flask under N_2 atmosphere and the reaction was kept at room temperature for three days. The polymerization was finally quenched by adding a small amount of hydrochloric acid. After synthesis, the reaction solution was diluted with anhydrous THF and precipitated with the excess of hexane. The collection was re-dissolved into dichloromethane and added to an excess amount of diethyl ether under vigorous stirring. The resulting copolymer was characterized by gel permeation chromatography (GPC) and the ^{1}H NMR spectroscopy.

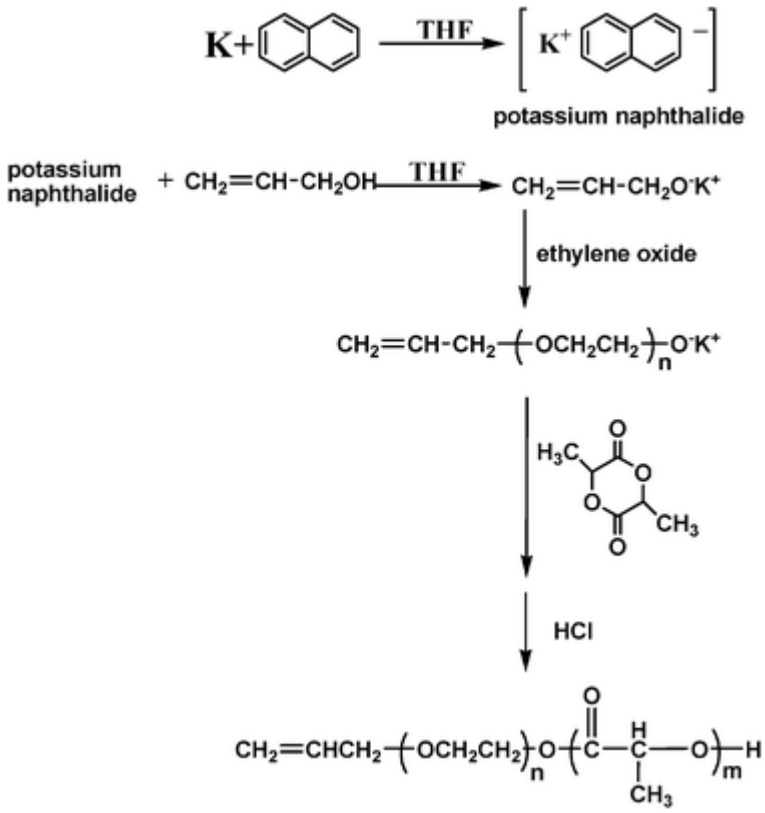

Scheme 2 Synthesis of allyl-PEG-PDLLA

copolymer.

Synthesis of hydrophobic SPIO nanoparticles

SPIO nanoparticles were prepared using the following procedures reported by Sun *et al.*[14] Briefly, iron(III) acetylacetonate (2 mmol), 1,2-hexadecanediol (10 mmol), oleic acid (6 mmol), oleylamine (6 mmol), and benzyl ether (20 ml) were mixed and magnetically stirred under a flow of nitrogen. The mixture was heated to 200 °C and maintained for 2 h. Then, it was heated to 300 °C to reflux for 1 h. The black-colored mixture was cooled to room temperature by removing the heat source. The black solution was then precipitated with ethanol and separated *via* centrifugation. After discarding the supernatant, the black product was dissolved in hexane in the presence of oleic acid and oleylamine. Centrifugation (6000 rpm, 10 min) was applied to remove the undispersed residue. The product, 6 nm Fe_3O_4 nanoparticles, was then precipitated with ethanol, centrifuged to remove the solvent, and redispersed into hexane.

Synthesis of hydrophilic SPIO nanoparticles

Hydrophilic SPIO nanoparticles were prepared for the MRI test, as this article will later discuss. A hexane dispersion of hydrophobic SPIO nanoparticles (40 mg in 0.2 ml) was added to a suspension of tetramethylammonium 11-aminoundecanoate in dichloromethane (40 mg in 2 ml). The mixture was shaken for 24 h. The resulting hydrophilic SPIO nanoparticles were collected using a magnet, washed with dichloromethane, and subsequently dispersed in deionized water.

Preparation of shell-cross-linked SPIO-DOX-loaded polymeric vesicles

The vesicle formation and the shell-cross-linked reaction were carried out simultaneously by a double-emulsion method. Typically, 0.2 ml water solution containing DOX (2 mg) and $K_2O_2S_8$ (0.1 mg, which is 1 wt% of the allyl-PEG-PDLLA copolymer amount) was added dropwise into 2 ml of a chloroform solution containing 10 mg allyl-PEG-PDLLA and 10 mg SPIO nanoparticles under sonication on ice (30 s). This primary emulsion was emulsified by sonication on ice in 4 ml 0.1% PVA aqueous solution. Subsequently, the resulting w/o/w emulsion was diluted by mixing with a 40 ml 0.5% PVA aqueous solution under vigorous stirring. After 2 min, the chloroform was evaporated using a rotary evaporator. The non-cross-linked SPIO-DOX-loaded vesicles formed were then centrifuged; after discarding the supernatant, the vesicles were resuspended in a water solution containing $K_2O_2S_8$ (the amount of $K_2O_2S_8$ in water was 1 wt% of the allyl-PEG-PDLLA copolymer amount). The resulting reaction mixture solution was initially bubbled for 30 min with N_2, subsequently heated to 50 °C under N_2, and then stirred for 5 h. After the reaction, the solution was dialyzed against water to remove the unencapsulated DOX and unreacted $K_2O_2S_8$. Finally, the vesicle solution was filtered with a 0.45 μm filter membrane to remove the large aggregates.

For the control experiment, we prepared the non-cross-linked SPIO-DOX-loaded vesicles using the same double emulsion method as described above.

Determination of the DOX and SPIO-loading contents

The DOX-loading content (DLC), defined as the weight percentage of DOX in SPIO-free vesicles, was quantified by UV-vis analysis using a Varian Cary model 100 Bio UV-vis spectrophotometer. First, SPIO-DOX-loaded vesicle solutions were lyophilized to yield the solid vesicle samples. Next, the dried vesicle samples were weighed and re-dissolved in a mixture of chloroform and DMSO (1 : 1, v/v). After the insoluble SPIO nanoparticles were removed from the solution by magnetic field-guided accumulation, the

absorbance of DOX at 480 nm was measured to determine the drug content in the solution using a previously established calibration curve. The loading density of SPIO nanoparticles inside the polymeric vesicles was determined using an atomic absorption spectrophotometer (AAS). Briefly, the freeze-dried vesicles were weighed and then added to 1 M HCl solution to allow the disaggregation of vesicles and complete dissolution of the SPIO nanoparticles. Iron concentration was determined at the specific Fe absorption wavelength (248.3 nm) based on a previously established calibration curve. The SPIO loading density was calculated as the ratio of iron oxide to the total weight of the vesicles.

Stability evaluation of the shell-cross-linked SPIO-DOX-loaded polymeric vesicles

The stability of the shell-cross-linked SPIO-DOX-loaded polymeric vesicles was evaluated using a Brookhaven BI-200SM laser scattering system equipped with multiple laser line filters at scattering angles between 15°–155° and with a wavelength of 532 nm. The experiments were performed at T = 25 °C and the samples were measured at different time periods. The hydrodynamic radius (R_h) and size distribution of the samples were determined by dynamic light scattering (DLS). For the static light scattering experiments, measurements were conducted at several finite angles and concentrations in order to obtain the radius of gyration (R_g) and the weight-average molecular weight of the shell-cross-linked vesicles *via* a Zimm plot.[12]

***In vitro* release of DOX from polymeric vesicles**

Freeze-dried vesicle samples were re-suspended in either PBS (pH 7.4) or ABS (pH 5.0) and transferred into a dialysis bag. The release study was performed at 37 °C in an incubator shaker. At selected time intervals, a sample (2 ml) of the buffered solution outside the dialysis bag was removed for UV-vis analysis and replaced with fresh buffered solution. The DOX concentration was calculated based on the absorbance intensity at 480 nm. The error bars were obtained from triplicate samples.

Confocal laser scanning microscopy (CLSM) analysis

CLSM analysis of a 1% (w/v) vesicle suspension was performed on a Leica Confocal Microscope equipped with a 488 nm Ar laser line for the dye excitation. The polymeric vesicle samples were prepared either with a hydrophobic fluorescent $DiOC_{18}$ dye loaded in the hydrophobic vesicle membrane or with DOX·HCl loaded in the inner aqueous core of the vesicle.

For cell uptake study, the 4T1 cells (1×10^6) were seeded onto 12 mm round glass coverslips placed in 24-well plates (Corning) and grown for 24 h. Cells were treated with DOX-loaded vesicles for 2 h (DOX concentration: 10 μg ml^{-1}). The cells were washed and fixed with 1.5% formaldehyde. Cover-slips were placed onto glass microscope slides and DOX uptake was imaged using a Leica TCS SP2 Confocal System installed on an upright compound microscope (Leica). Digital monochromatic images were acquired using Leica Confocal Software (Version 2.61) under identical conditions.

***In vitro* cytotoxicity study**

The cytotoxicity of the SPIO-DOX-loaded vesicles against 4T1 cells was studied using the MTT assay. First, 4T1 cells (1×10^4) were seeded in 96-well plates and incubated for 24 h. The media was replaced with fresh media containing free DOX, shell-cross-linked or non-cross-linked SPIO-DOX-loaded vesicles (DOX concentration: 10 μg ml^{-1}) or control media and incubated for 48 h. Thereafter, the wells were washed three times with warm phosphate buffer solution and incubated again for another 3 h with RPMI containing 250 μg mL^{-1} of MTT. After discarding the culture medium, 200 μL of DMSO was added to dissolve the precipitates and the resulting solution was measured for absorbance at 570 nm with a reference wavelength of 690 nm using a microplate reader (Molecular Devices).

Relaxivity measurement

T_1 and T_2 relaxivities were measured at 1.5 T on a clinical MR scanner (Philips Intera) at room temperature. The T_2-weighted images were acquired using the following parameters: TR/TE, 2600/100 ms; FOV, 150 mm; matrix, 256 × 256; slice thickness, 1.5 mm. T_2-weighted images were acquired with a conventional spin-echo acquisition with TE values ranging from 11 to 90 ms. The relaxivity values, r_1 and r_2, were calculated through the linear least-squares curve fitting of 1/relaxation time (s^{-1}) *versus* the iron concentration (mM Fe).

Results and discussion

Polymeric vesicles were prepared using biodegradable amphiphilic diblock copolymers with allyl functional end groups, *i.e.*, allyl-poly(ethylene glycol)-poly(D,L-lactide) (allyl-PEG-PDLLA) (Scheme 2). This copolymer was synthesized through sequential anionic ring-opening polymerization of ethylene oxide (EO) and D,L-lactide in one pot, using potassium alkoxide as an initiator. First, we prepared allyl-terminated PEG using allyl alkoxide as an initiator during anionic polymerization of EO and subsequently prepared the allyl-PEG-PDLLA copolymer by a ring-opening anionic polymerization of D,L-lactide using allyl-terminated PEG as an initiator. This stepwise, anionic ring-opening polymerization was performed in a well-controlled manner with regard to the copolymer molecular weight as well as the length of individual blocks. The feed ratio was controlled to achieve the final copolymer composition (allyl-PEG2k-PDLLA14k, the hydrophilic PEG volume fraction f_{EO}~ 0.11, Fig. 1). The lengths of the PEG and PDLLA blocks were calculated by comparing the integrals of the characteristic peaks of PEG (*e.g.*, the singlet of –CH_2–O– at 3.65 ppm) and PDLLA (*e.g.*, the multiplet of –CH(CH_3)–O– at 1.5 ppm) with that of the characteristic peaks of the terminal allyl groups (*e.g.*, the multiplet of CH_2?C*H*– at 5.9 ppm) in the ^{1}H NMR spectroscopy. The molecular weight of the copolymer (M_w) was 18?038, as determined by GPC.

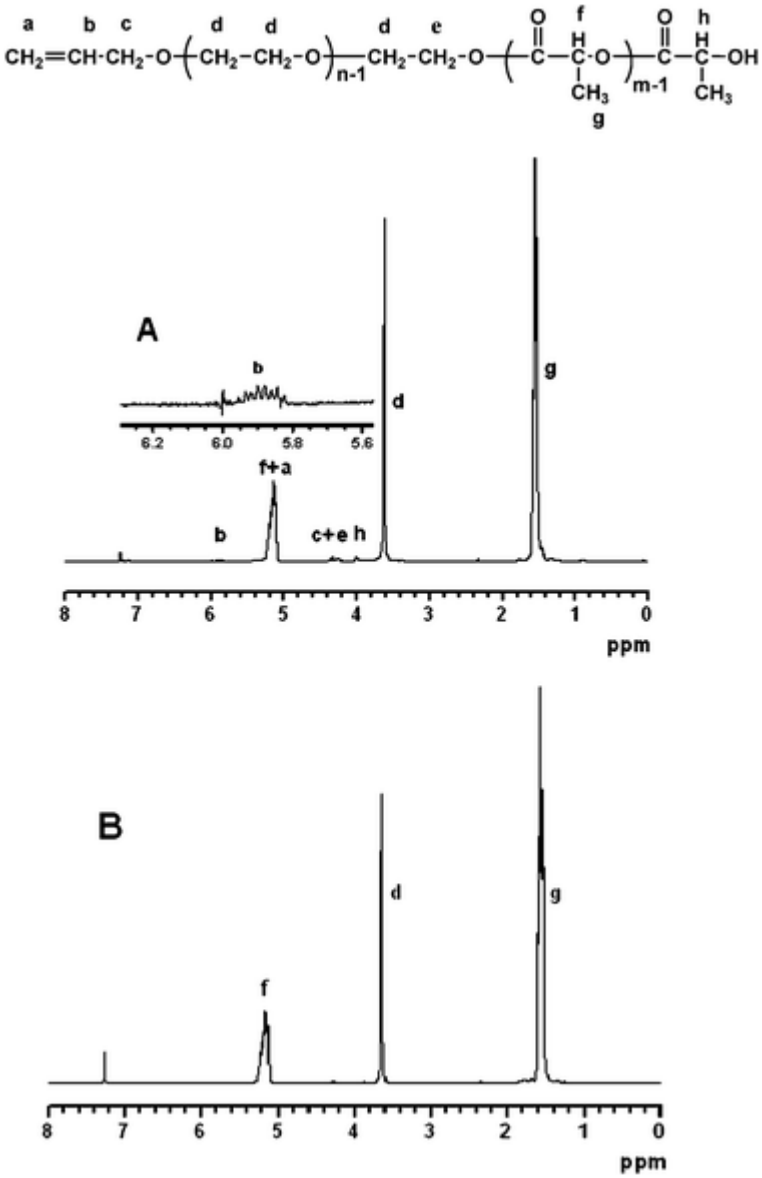

Fig. 1 ^{1}H NMR spectra of the freeze-dried vesicle powder before (a) and after (b) the shell-cross-linked reaction based on PEG and PDLLA block copolymers.

Extensive theoretical[15,16] and experimental studies have established that amphiphilic block copolymers can self-assemble into various types of nanostructures such as micelles and vesicles determined by a number of factors, including the molecular structure of the copolymers and the type of self-assembly process employed.[17–20] In this study, we used the emulsion/solvent evaporation technique to form polymeric vesicles from the allyl-PEG2k-PDLLA14k copolymer. First, quantified water (the aqueous inner phase) containing DOX and $K_2O_2S_8$ (as a cross-linking initiator for the inner hydrophilic layer) was emulsified in a chloroform solution (the intermediate organic/oil phase) containing the copolymers and SPIO nanoparticles under sonication. This primary emulsion was further emulsified by sonication on ice in a 0.1% polyvinyl alcohol (PVA) aqueous solution (the aqueous outer phase). The water/oil/water emulsion obtained was diluted into an excess of 0.5% PVA aqueous solution under rapid magnetic stirring. Then, the chloroform was evaporated using a rotary evaporator and the polymeric vesicles were formed. Consequently, SPIO nanoparticles were loaded into the vesicles' membrane and DOX was encapsulated into the inner aqueous core at 47.2 and 4.5

wt.%, respectively. Both SPIO and DOX loading in this polymeric vesicle system were higher than that in polymeric micelles using the similar diblock copolymers.[21]

We investigated various approaches to achieve the shell-cross-linked vesicles and to control the size of the vesicles. Direct core cross-linking of PEG-*b*-PDLLA micelles was achieved successfully in an aqueous micellar solution by Kataoka *et al.* using either inorganic or organic initiators for radical polymerization.[22,23] In light of their success, we attempted to directly cross-link the hydrophilic shells of the vesicles in the aqueous vesicle solution. The radical polymerization was initiated at elevated temperatures (50 °C) using $K_2O_2S_8$. To ensure a complete reaction, the reaction mixture was analyzed *via* ^{1}H NMR spectroscopy periodically during the reaction until the double bond in the allyl groups disappeared completely (see Fig. 1a and b). We found no change in the average dimensions and the polydispersity of the vesicles upon polymerization according to the dynamic light scattering (DLS) analysis; thus, the potential cross-linking reaction between different vesicles did not occur notably. This is most likely due to the steric hindrances as well as different electron densities of the double bond in allyl-PEG-PDLLA.

Hydrophobic SPIO nanoparticles were synthesized with precise control of the particle diameter (6 nm), following a published procedure by Sun *et al.*[14] Fig. 2a shows the TEM image of the SPIO nanoparticles with a uniform in size distribution. These SPIO nanoparticles are covered with hydrophobic aliphatic chains from oleic acid and oleylamine during synthesis, which is essential for vesicle encapsulation in the hydrophobic membrane. Fig. 2b and 2c show the morphology of double shell-cross-linked DOX-loaded vesicles (SPIO free) and SPIO-DOX-loaded vesicles. Fig. 2b clearly demonstrates that the preparation procedure yielded spherical hollow vesicles with a hydrophobic membrane evidenced by the contrast. The diameter of the polymeric vesicles was about 220 nm. Fig. 2c revealed that a large number of individual SPIO nanoparticles were incorporated uniformly into the hydrophobic membrane of the shell-cross-linked vesicles and the diameter of the SPIO-DOX-loaded vesicles was about 230 nm. These SPIO nanoparticles formed a cluster in the polymeric vesicle.

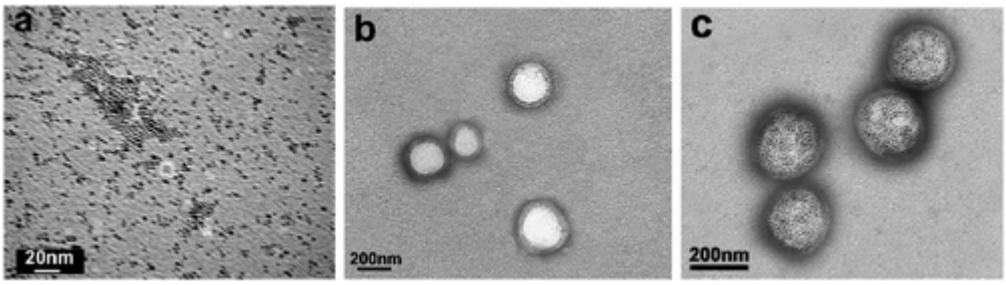

Fig. 2 Transmission electron microscopy (TEM) images of (a) 6 nm hydrophobic SPIO nanoparticles; (b) DOX-loaded (SPIO free) and (c) SPIO-DOX-loaded shell-cross-linked vesicles.

The size and size distribution of the polymeric vesicles in aqueous solution were analyzed by DLS. The mean hydrodynamic diameter of a DOX-loaded shell-cross-linked vesicle was 231 ± 3 nm (Fig. 3a), the polydispersity was 0.107 ± 0.003; while the mean hydrodynamic diameter was 240 ± 2 nm (Fig. 3b) and the polydispersity was 0.115 ± 0.002 for SPIO-DOX-loaded shell-cross-linked vesicles. The slight increase in diameter for the SPIO-DOX-loaded vesicles compared with that of the DOX-loaded vesicles may be attributed to the incorporation of a large amount of SPIO nanoparticles (47.2%) resulting from a favorable interaction between SPIO nanoparticles and the hydrophobic membrane of the vesicles.

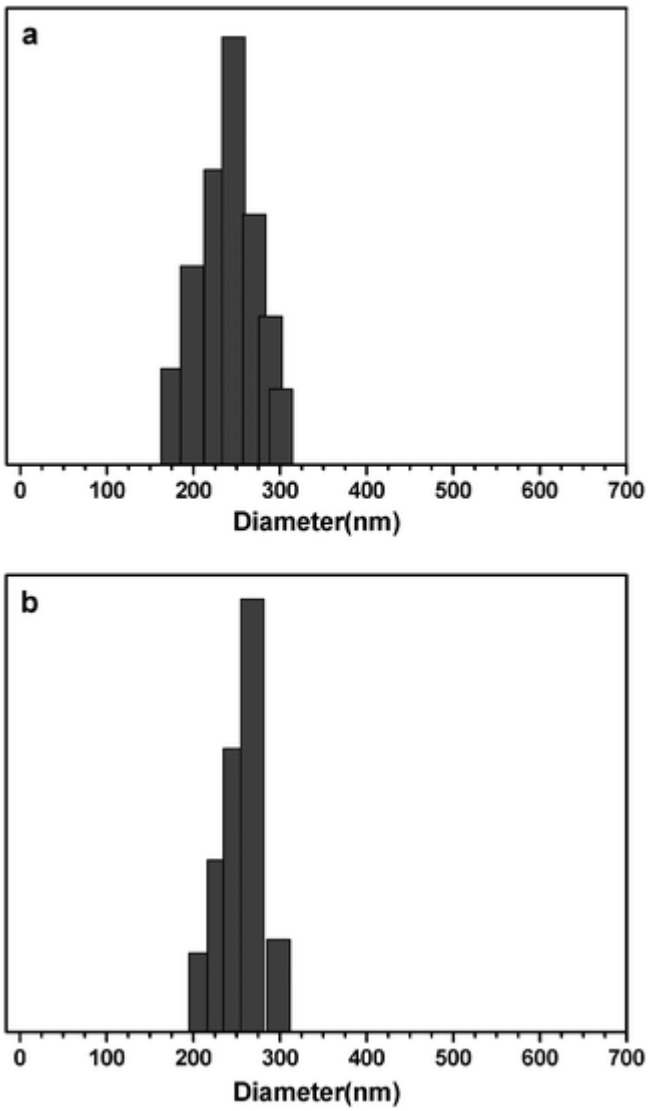

Fig. 3 Dynamic light scattering (DLS) histogram of DOX-loaded (a) and SPIO-DOX-loaded vesicles (b) based on shell-cross-linked copolymers.

To further analyze the morphology of vesicles using CLSM, we incorporated either a hydrophobic green fluorescent probe ($DiOC_{18}$) or a hydrophilic red fluorescent probe (DOX) into the hydrophobic membrane or the inner aqueous core of the shell-cross-linked vesicles, respectively, to investigate the formation and loading capability of the vesicles. Fig. 4a shows the CLSM images of the hydrophobic fluorescent $DiOC_{18}$ loaded vesicles, which clearly indicate that vesicles were successfully formed using the emulsion/solvent evaporation technique. Moreover, these vesicles were unilamellar hollow spheres and the size and size distribution were consistent with the TEM and DLS findings, as reported earlier. Fig. 4b shows the CLSM images of the stable DOX-loaded vesicles.

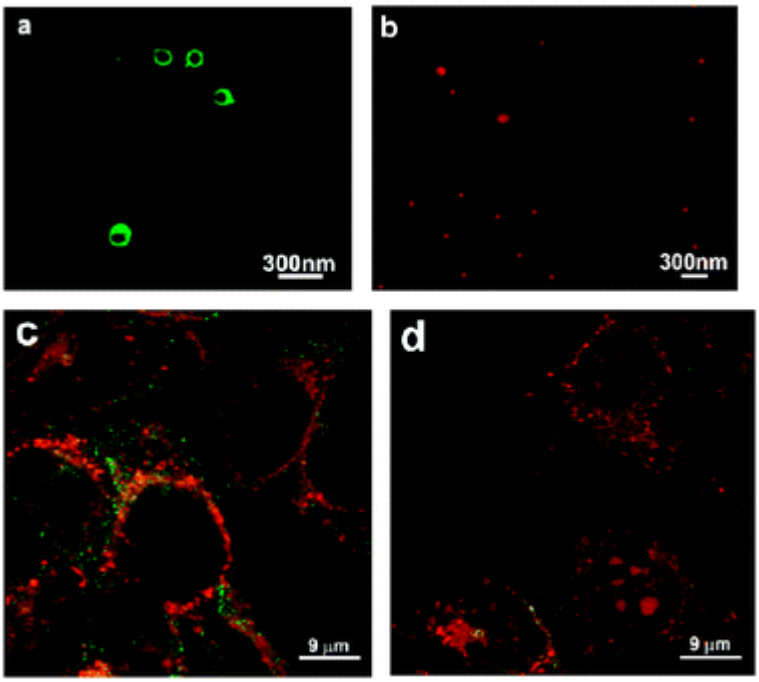

Fig. 4 CLSM images of (a) hydrophobic fluorescent $DiOC_{18}$ loaded shell-cross-linked vesicles; (b) DOX-loaded shell-cross-linked vesicles; (c) 4T1 cells treated with shell-cross-linked SPIO-DOX-loaded vesicles and fluorescent transferrin; (d) 4T1 cells treated with non-cross-linked vesicles and fluorescently labeled transferrin (incubation time: 2 h).

CLSM was also used to study the uptake of shell-cross-linked and non-cross-linked SPIO-DOX-loaded vesicles by 4T1 cells. To investigate the subcellular distribution of these vesicles, we marked the endosomes with fluorescently labeled transferrin, which reportedly traffics specifically through the endocytic recycling compartment.[24] As shown in Fig. 4 (c and d), once taken up by the cells, we observed punctuate localization of both vesicles (*i.e.*, DOX fluorescence) and the fluorescent transferrin, indicating that all were located in the cytoplasm. Importantly, we did not observe colocalization of vesicles and transferrin indicating that these were not taken up into the same endosomes. This is expected since transferrin will be taken up *via* receptor-mediated endocytosis while the vesicles are most likely taken up *via* macropinocytosis. For the shell-cross-linked vesicles, the majority of the DOX fluorescence was observed within the cytoplasm with little to no nuclear staining (Fig. 4c). In contrast, for the non-shell-cross-linked vesicles there was more diffuse cytoplasmic DOX fluorescence and a significant amount of nuclear DOX staining (Fig. 4d). This result suggests there is a greater drug release from the non-cross-linked vesicles after the 2 h incubation, resulting in DOX diffusion into the cytoplasm and more nuclear DOX staining. These results are consistent with the *in vitro* drug release profile of these two different vesicles.

The stability of the shell-cross-linked SPIO-DOX-loaded vesicles was evaluated using both DLS and SLS at different time periods. Table 1 shows the results of the DLS and SLS analysis. The shell-cross-linked SPIO-DOX-loaded vesicles did not display any notable changes in the size and size distribution during the entire period (*i.e.*, 18 days) monitored; thus, they are very stable. Furthermore, the molecular weight and radius of gyration of the shell-cross-linked vesicles were evaluated using the static light scattering technique, which also did not reveal any notable change.[12]

Table 1 Results from dynamic and static light scattering experiments performed on shell-cross-linked SPIO-DOX-loaded vesicles

Formulation	M_w (10^7 g mol^{-1})			R_g (nm)			R_h (nm)		
Shell-cross-linked SPIO-DOX-loaded vesicles in water	6 days	12 days	18 days	6 days	12 days	18 days	6 days	12 days	18 days
	6.8 ± 0.2	6.5 ± 0.3	6.6 ± 0.3	242 ± 3	239 ± 2	240 ± 3	238 ± 2	235 ± 3	237 ± 2

Polydispersity			? (R_g/R_h)		
6 days	12 days	18 days	6 days	12 days	18 days
0.109 ± 0.002	0.117 ± 0.004	0.115 ± 0.005	1.017 ± 0.006	1.017 ± 0.007	1.013 ± 0.005

The release behavior of SPIO-DOX-loaded shell-cross-linked vesicles and that of SPIO-DOX-loaded non-shell-cross-linked vesicles was investigated at two pH values (7.4 and 5.0). As shown in Fig. 5, for non-shell-cross-linked vesicles, the DOX release revealed a distinct biphasic release pattern consisting of an initial burst release followed by a sustained and slow release up to a couple of days. No burst release behavior was observed for shell-cross-linked vesicles; thus, the inner and outer shell-cross-linked hydrophilic PEG layers may suppress the burst release behavior. In addition, DOX-release from both cross-linked and non-cross-linked vesicles at pH 5.0 was faster than that at pH 7.4. This is likely due to the faster degradation of vesicles at lower pH. Drug release in shell-cross-linked vesicles was somewhat faster after four days, possibly due to the gradual degradation within the hydrophobic PDLLA membrane and at the inner and outer PEG-polyester interfaces.

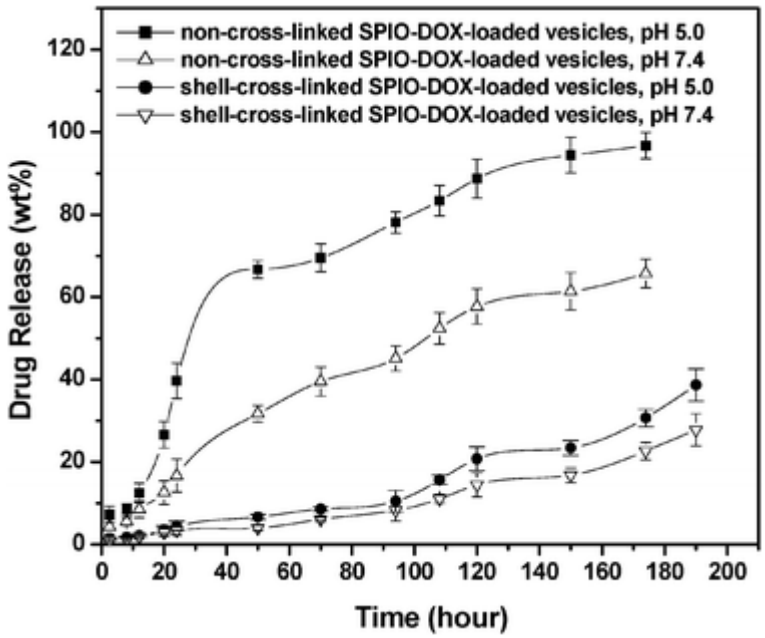

Fig. 5 *In vitro* SPIO-DOX-release profiles of non-shell-cross-linked and shell-cross-linked vesicles at different pH (pH 5.0 and 7.4) at 37 °C (the error bars were obtained from triplicate samples).

Fig. 6 shows the cytotoxic effect of free DOX, shell-cross-linked and non-shell-cross-linked SPIO-DOX-loaded vesicles against 4T1 cancer cells after incubation for 48 h. The cell viability in the presence of shell-cross-linked vesicles was much higher than that of non-shell-cross-linked vesicles because the DOX release was significantly slower from that of the shell-cross-linked vesicles due to their cross-linked hydrophilic shells compared with the non-shell-cross-linked vesicles. However, the shell-cross-linked structure will provide superior stability *in vivo* and can potentially reduce the rapid clearance of SPIO-DOX-loaded vesicles from the blood stream after their intravascular administration. In the presence of free DOX, the cell viability of cells was dramatically decreased, which may be attributed to the fast diffusion of free DOX into the cells.

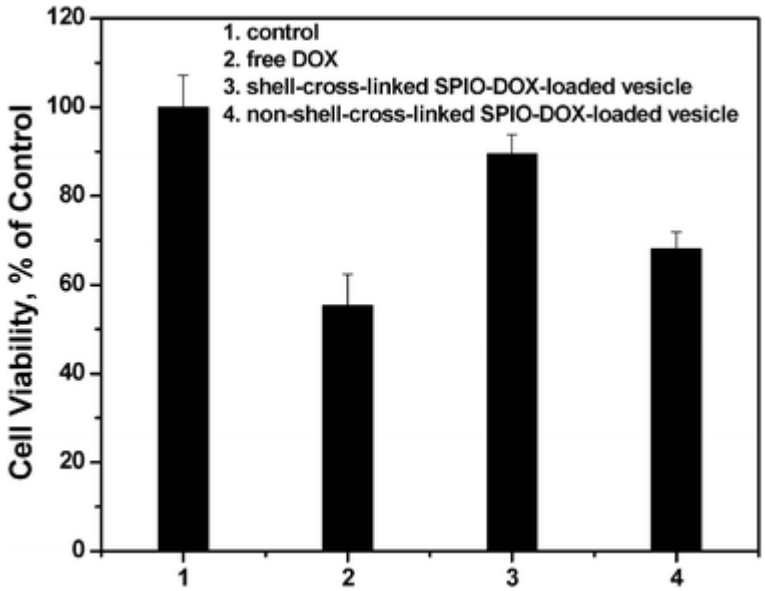

Fig. 6 Cytotoxicity study of free DOX, shell-cross-linked and non-shell-cross-linked SPIO-DOX-loaded vesicles against 4T1 cells after incubation for 48 h.

The relaxation times T_1 (spin–lattice relaxation) and T_2 (spin–spin relaxation) were measured on a clinical 1.5 T MRI scanner. The efficiency of MRI contrast agent is commonly assessed in terms of its relaxivities, $r_1$and r_2, which were calculated through linear least squares fitting of the 1/relaxation time (s^{-1}) *versus* the iron concentration (mM Fe), as shown in Fig. 7A. For a T_2 contrast agent, the higher the r_2/r_1, the better the contrast efficacy. Table 2 summarizes the relaxivities of SPIO-loaded polymeric vesicle and hydrophilic SPIO nanoparticles. The r_2/r_1 ratio value of the SPIO-loaded polymeric vesicle was approximately 13 times higher than that of the hydrophilic SPIO nanoparticles, and was also 12 times higher than that of a commercially available T_2 agent Resovist® (r_2/r_1 = 5.9 as reported in the manufacturer's technical data sheet), indicating that the SPIO-loaded polymeric vesicles can serve as a highly efficient T_2 contrast agent. Resovist® consists of SPIO nanoparticles coated with carboxydextran and is mostly used for the detecting and characterizing especially small focal liver lesions.[25]

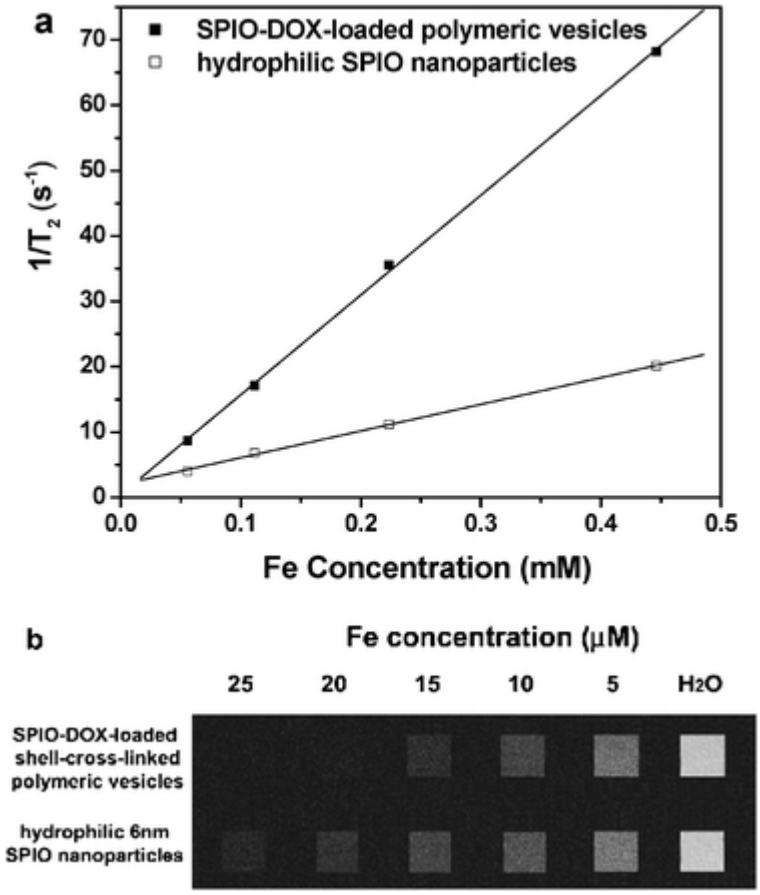

Fig. 7 (a) T_2 relaxation rates ($1/T_2$, s^{-1}) as a function of iron concentration (mM) for hydrophilic SPIO nanoparticles and SPIO-DOX-loaded shell-cross-linked polymeric vesicles. (b) T_2-weighted MRI images of the above two formulations.

Table 2 SPIO nanoparticle loading level, T_1 and T_2 relaxivities (r_1 and r_2), and MRI sensitivity for different formulations

Formulation	SPIO loading (wt%)	r_1	r_2	r_2/r_1	MRI sensitivity/μg ml^{-1}
6 nm SPIO-DOX-loaded polymeric vesicle	47.2	2.1	152.7	72.7	2.9
6 nm hydrophilic SPIO nanoparticles	—	7.6	40.8	5.4	—
Resovist®	—	25.4	151.0	5.9	—

Note, r_1 and r_2 values are in the unit of Fe mM^{-1} s^{-1}.

Note, r_1 and r_2 values are in the unit of Fe mM^{-1} s^{-1}.

It has been reported that the T_2 relaxation rate of ice is very high.[26] In an aqueous medium, the mobility of the water molecules located in the hydrophilic shells of the SPIO-loaded polymeric vesicles is restricted due to the formation of hydrogen bonds between the water molecules and the hydrophilic PEG blocks, resulting in a large amount of "icelike" water;[27] Therefore, the large T_2 relaxivity (r_2) of SPIO-loaded polymeric vesicles is a result of "icelike" water in the hydrophilic shells. Moreover, the formation of SPIO nanoparticle

clusters in the hydrophobic membranes of the SPIO-loaded polymeric vesicles can also greatly enhance the r_2 value. In contrast, the T_1 relaxivity (r_1) of the SPIO-loaded polymeric vesicle was significantly lower than that of the hydrophilic SPIO nanoparticles or Resovist® (*cf.*Table 2) because the water molecules diffused into the PEG domains hardly come into contact with the SPIO nanoparticles encapsulated in the hydrophobic membranes of the vesicles, which in turn kinetically limits the spin–lattice relaxation rate. As a result, the r_2/r_1 ratio of the SPIO-loaded polymeric vesicle was much higher than that of the hydrophilic SPIO nanoparticles or Resovist®.

To evaluate the effect of SPIO nanoparticle clustering on the MRI images, we compared the MRI signal intensities between the hydrophilic SPIO nanoparticles and the SPIO-loaded vesicles. As shown in Fig. 7B, for a given Fe concentration, the vesicles showed a significantly darker (T_2-weighted) image than the hydrophilic SPIO nanoparticles dispersed in water, confirming that SPIO nanoparticle clustering drastically increased the image contrast. Furthermore, to quantify the MRI sensitivity of the SPIO-loaded polymeric vesicles, the MRI detection limit of the SPIO-loaded polymeric vesicles is defined as the vesicle concentration at which the MRI signal intensity decreases to 50% of that for pure water in T_2-weighted images. The MRI detection limit of the SPIO-loaded vesicles prepared in this study was 2.9 μg ml^{-1}, which was much lower than that of the reported SPIO-loaded polymeric micelles (20.5 μg ml^{-1}).[10]

Conclusion

Multifunctional polymeric vesicles were developed based on the amphiphilic copolymer allyl-PEG-PDLLA. SPIO nanoparticles and DOX were simultaneously loaded into the hydrophobic membrane and the hydrophilic aqueous core of the polymeric vesicles, respectively. The SPIO-loaded vesicles showed a much higher r_2/r_1 ratio than SPIO nanoparticles and a commercial MRI contrast agent, Resovist®. Moreover, to enhance the stability of the polymeric vesicles during blood circulation, both the inner and outer hydrophilic PEG shells were cross-linked by polymerization of the PEG end groups. Thus, these highly-stable SPIO-DOX-loaded polymeric vesicles can serve as ultrasensitive MRI probes while simultaneously delivering therapeutic agents to the target tissues, thereby making cancer theranostics possible.

Acknowledgements

We acknowledge the financial support for this project from the University of Wisconsin-Milwaukee.

References

1 Y. Bae, W. Jang, N. Nishiyama, S. Fukushima and K. Kataoka, *Mol. BioSyst.*, 2005, **1**, 242.
2 S. F. Chin, K. Swaminathan Iyer, C. L. Raston and M. Saunders, *Adv. Funct. Mater.*, 2008, **18**, 922.
3 X. Y. Shi, S. H. Wang, S. D. Swanson, S. Ge, Z. Y. Cao, M. E. Van Antwerp, K. J. Landmark and J. R. Baker, *Adv. Mater.*, 2008, **20**, 1671.
4 M. J. Alonso, *Biomed. Pharmacother.*, 2004, **58**(3), 168.
5 D. Peer, J. M. Karp, S. Hong, O. C. Farokhzad, R. Margalit and R. Langer, *Nat. Nanotechnol.*, 2007, **2** (12), 751.
6 Y. Ding, Y. Hu, X. Jiang, L. Zhang and C. Yang, *Angew. Chem., Int. Ed.*, 2004, **43**(46), 6369.
7 J. H. Lee, Y. M. Huh, Y. W. Jun, J. W. Seo, J. T. Jang, H. T. Song, S. J. Kim, E. J. Cho, H. G. Yoon, J. S. Suh and J. W. Cheon, *Nat. Med.*, 2007, **13**, 95.
8 E. S. Lee, H. J. Shin, K. Na and Y. H. Bae, *J. Controlled Release*, 2003, **90**(3), 363.
9 E. S. Lee, H. J. Shin, K. Na and Y. H. Bae, *J. Controlled Release*, 2005, **103**(2), 405.
10 H. Ai, C. Flask, R. Weinberg, X. Shuai, M. Pagel, D. Farrell, J. Duerk and J. Gao, *Adv. Mater.*, 2005, **17**, 1949.
11 N. Nasongkla, E. Bey, J. Ren, H. Ai, C. Khemtong, J. S. Guthi, S. F. Chin, A. D. Sherry, D. A. Boothman and J. Gao, *Nano Lett.*, 2006, **6**(11), 2427.

12 C. Nardin, T. Hirt, J. Leukel and W. Meier, *Langmuir*, 2000, **16**, 1035.

13 A. Harada and K. Kataoka, *Prog. Polym. Sci.*, 2006, **31**, 949.

14 S. Sun, H. Zeng, D. B. Robinson, S. Ranous, P. M. Rice, S. Wang and G. Li, *J. Am. Chem. Soc.*, 2004, **126**, 273.

15 F. S. Bates, *Science*, 1991, **251**, 898.

16 F. S. Bates and G. H. Fredrickson, *Phys. Today*, 1999, **52**(2), 32.

17 R. Gref, Y. Minamitae, M. T. Peracchia, V. Trubetskoy and V. Torchillin, *Science*, 1994, **263**, 1600.

18 K. Avgoustakis, A. Beletsi, Z. Panagi, P. Klepetsanis, A. G. Karydas and D. S. Ithakissios, *J. Controlled Release*, 2002, **79**(1–3), 123.

19 K. Yasugi, T. Nakamura, Y. Nagasaki, M. Kato and K. Kataoka, *Macromolecules*, 1999, **32**, 8024.

20 H. K. Kim and T. G. Park, *Macromol. Rapid Commun.*, 2002, **23**, 26.

21 X. Yang, Y. Chen, R. Yuan, Z. Xiao, D. Quan, G. Chen, E. Blanco, J. Gao and X. Shuai, *Polymer*, 2008, **49**, 3477.

22 K. Emoto, Y. Nagasaki and K. Kataoka, *Langmuir*, 1999, **15**, 5212.

23 M. Iijima, Y. Nagasaki, T. Okada, M. Kato and K. Kataoka, *Macromolecules*, 1999, **32**, 1140.

24 M. Zhang, A. Haapasako, D. Y. Kim, L. A. MacKenzie Ingano, W. H. PettingeII and D. M. Kovace, *FASEB J.*, 2006, **20**, E271.

25 http://www.bayerscheringpharma.de/scripts/pages/en/index.php.

26 J. G. Georgiadis and M. Ramaswamy, *Int. J. Heat Mass Transfer*, 2005, **48**, 1064.

27 J. Qin, S. Laurent, Y. S. Jo, A. Roch, M. Mikhaylova, Z. M. Bhujwalla, R. N. Muller and M. Muhammed, *Adv. Mater.*, 2007, **19**(14), 1874.